Hindawi
Shock and Vibration
Volume 2017, Article ID 5161870, 10 pages
https://doi.org/10.1155/2017/5161870

Research Article

Impact Dynamics of a Percussive System Based on Rotary-Percussive Ultrasonic Drill

Yinchao Wang, Qiquan Quan, Hongying Yu, He Li, Deen Bai, and Zongquan Deng

State Key Laboratory of Robotics and System, Harbin Institute of Technology, No. 92, Xidazhi Street, Nangang District, Harbin 150001, China

Correspondence should be addressed to Qiquan Quan; quanqiquan@hit.edu.cn

Received 3 June 2017; Accepted 23 August 2017; Published 9 October 2017

Academic Editor: Dario Di Maio

This paper presents an impact dynamic analysis of a percussive system based on rotary-percussive ultrasonic drill (RPUD). The RPUD employs vibrations on two sides of one single piezoelectric stack to achieve rotary-percussive motion, which improves drilling efficiency. The RPUD's percussive system is composed of a percussive horn, a free mass, and a drill tool. The percussive horn enlarges longitudinal vibration from piezoelectric stack and delivers the vibration to the drill tool through the free mass, which forms the percussive motion. Based on the theory of conservation of momentum and Newton's impact law, collision process of the percussive system under no-load condition is analyzed to establish the collision model between the percussive horn, the free mass, and the drill tool. The collision model shows that free mass transfers high-frequency small-amplitude vibration of percussive horn into low-frequency large-amplitude vibration of drill tool through impact. As an important parameter of free mass, the greater the weight of the free mass, the higher the kinetic energy obtained by drill tool after collision. High-speed camera system and drilling experiments are employed to validate the inference results of collision model by using a prototype of the RPUD.

1. Introduction

As rock samples of asteroid are rich in geological information, which contributes to getting a deeper understanding on the origin of the universe, acquiring rock samples is now an important target in space exploration projects. Drilling is an important method for rock samples collection [1–4]. In the existing sample drilling devices, ultrasonic drill is a kind of sampling device which can drill into the rocks under low weight on bit and low power consumption. Therefore, the ultrasonic drill has wider application prospect in space sampling under low-gravity environments [5].

The developing process of the ultrasonic drill can be divided into two stages. In the initial stage, ultrasonic drill only has an impact function to break rocks, such as Ultrasonic/Sonic Driller/Corer (USDC) [6–8], Ultrasonic Drill Tools (UDT) [9], and Ultrasonic/Sonic Driller (USD) [10]. Late development of the ultrasonic drill adds with rotary function or torsional function [11] to improve drilling efficiency, such as Auto-Gopher [12, 13], Percussive Augmenter of Rotary Drills (PARoD) [14], Ultrasonic Planetary Core Drill (UPCD) [15, 16], and Single Piezo-Actuator Rotary-Hammering Drill (SPaRH) [17]. The typical representative of the initial stage of ultrasonic drill is USDC, which consists of four parts: a piezoelectric transducer, a tuned horn, a free mass, and a drill tool. Tuned horn amplifies the vibration generated from piezoelectric transducer and delivers impact motion to the drill tool through free mass. USDC can quickly break into the rocks depending on the impact motion. Though impact motion is helpful to remove drilling chips in a certain extent, it is difficult to achieve chips removal effectively, especially when drilling to a certain depth. Torsional ultrasonic drill utilizes ultrasonic horn to generate longitudinal-torsional vibration to improve the drilling chips removal efficiency. However, the improvement of drilling efficiency is limited; the chips removal efficiency still needs to be improved. According to the difference of power mode, rotary ultrasonic drill can be divided into two types: motor-rotary and piezoelectric-rotary. Motor-rotary ultrasonic drill uses electromagnetic motor to rotate the

drill tool to remove drilling chips, which raises the drilling efficiency effectively. Nevertheless, adding a motor to the ultrasonic drill may increase the degree of drilling, which also brings complication to the power supply. Piezoelectric-rotary ultrasonic drill utilizes piezoelectric ceramics as the rotary and impact power, which has a more compact system structure and stronger environmental adaptability compared with motor-rotary ultrasonic drill. SPaRH is a representative of the piezoelectric-rotary ultrasonic drill, which consists of four parts: a piezoelectric transducer, a grooved horn, a keyed free mass, and a drill tool. The grooved horn translates longitudinal vibration of the piezoelectric transducer into longitudinal-torsional vibration. After receiving vibration from the horn, the keyed free mass makes the drill tool realize rotary-impact motion. However, as the rotary motion and impact motion of SPaRH are coupled together, it is difficult to adjust the rotation or impact parameters separately, which may limit the scope of application of SPaRH.

As is well known, the piezoelectric ceramics transmit vibration to both sides. The existing ultrasonic drill only uses the vibration on front side, and part of vibration on the back side is not used. In our previous work, a rotary-percussive ultrasonic drill (RPUD) based on one single piezoelectric transducer is proposed to drill into rocks in rotary-percussive motion, which uses the vibration energy on both sides of the piezoelectric ceramics [18]. Drilling experiment shows that the RPUD can raise the drilling efficiency of rock sampling.

To validate the energy delivering capability of the percussive system, the dynamic analysis of impact between the percussive horn, the free mass, and the drill tool needs to be carried out. Nowadays, the research on the collision process of percussive system can be divided into theoretical research and experimental research. In the research of [8], integrated modeling method and finite element method are employed to analyze the impact contact between the ultrasonic horn and the free mass. But, there is no research on collision of the drill tool. According to the study of [19, 20], it is assumed that the drill tool is fixed and the ultrasonic horn can move axially, and set-oriented method is chosen to analyze the drilling system with contact interfaces. However, there is lack of experiments to validate the collision model. Based on the paper of [21], a drill rod is assumed to be consolidated with rock, solid body collision is used to analyze ultrasonic horn and free mass, and free mass and drill rod impact process, and the drill rod model for both undamped and damped states is discussed. And a spherical mass is studied only through experiment by the study of [22]. The effects of multiple free mass and single free mass on the impact force are tested through ultrasonic drilling experiments.

Above all, to the best knowledge of the authors, the research about the collision process of the free mass is mostly in the load condition of the ultrasonic drill, which means that ultrasonic drill breaks into rocks and the drill tool is fixed with the rocks. In order to describe the collision process of the free mass unit intuitively and clearly and eliminate the interference factors, this paper analyzes the free mass collision process under no-load condition. In this paper, the collision process of the percussive system is studied based on the RPUD. Using Newton's impact law, the collision model of percussive horn, free mass, and drill tool is established. As the weight of free mass has a significant effect on the energy transfer process, based on the collision model, the effect of weight of free mass on the kinetic energy of drilling tool under no-load condition is discussed as well. To verify the collision model, the vibration process of the percussive system under no-load condition is observed through high-speed camera. Motion parameters of free mass are extracted and analyzed. Moreover, the effect of weight of free mass on the kinetic energy of drilling tool is verified. In order to further confirm the validity of the collision model, the drilling experiments under load condition is carried out based on the RPUD.

The remaining sections of the paper are organized as follows. In Section 2 the structure and working principle of the RPUD are proposed. Section 3 presents a collision model of percussive system under no-load condition, including the collision model of the free mass with percussive horn and drill tool. In Section 4, the simulation of collision model is presented. High-speed camera system and drilling experiments are employed to evaluate the collision performance in Section 5. Finally, Section 6 concludes this paper.

2. Structure and Working Principle

The RPUD is proposed based on the vibration of piezoelectric ceramics on both sides. RPUD consists of PZT (piezoelectric ceramics of $PbZrO_3$-$PbTiO_3$ system) ceramics, a rotary unit, a percussive unit, a sleeve, and a drill tool, as shown in Figure 1(a). PZT ceramics are composed of four piezoelectric ceramics and placed between rotary unit and percussive unit.

The rotary unit is located on the back of the PZT ceramics and consists of a V type of longitudinal-torsional vibration coupling element (V-LT coupler) [23], a rotor, and a preload spring. The bottom of the V-LT coupler is connected to the PZT ceramics by bolts. The rotor is engaged with the driving teeth of the V-LT coupler and the preload force is provided by the preload spring. The percussive unit is connected with the front of the PZT ceramics and is composed of a percussive horn, a free mass, and a restoring spring. The same as V-LT coupler, the bottom of the percussive horn is linked with the PZT ceramics by bolts as well. The free mass is fitted with the top of the percussive horn and the preload force is provided by the restoring spring, as shown in Figure 1(b). The drill tool is composed of a spiral drill pipe and a drilling bit. The percussive horn, the free mass, and the drill tool constitute the percussive system of the RPUD. Preload force on the rotor is about 18 N, and the preload force on the free mass is about 5 N. The mass of the RPUD is about 590 g.

Based on the composition of RPUD system, ANSYS (ANSYS12.0, ANSYS Inc., Canonsburg, PA, USA) [24] is employed to establish the finite element model of the V-LT coupler and percussive horn (rotary-percussive composition), as shown in Figure 2. The PZT ceramics use d_{33} working mode for the excitations of longitudinal vibration and are polarized along their thickness directions. Figure 3 gives the vibration shape and displacement vector of the rotary-percussive composition in modal analysis, respectively. When the rotary-percussive composition works in resonant state,

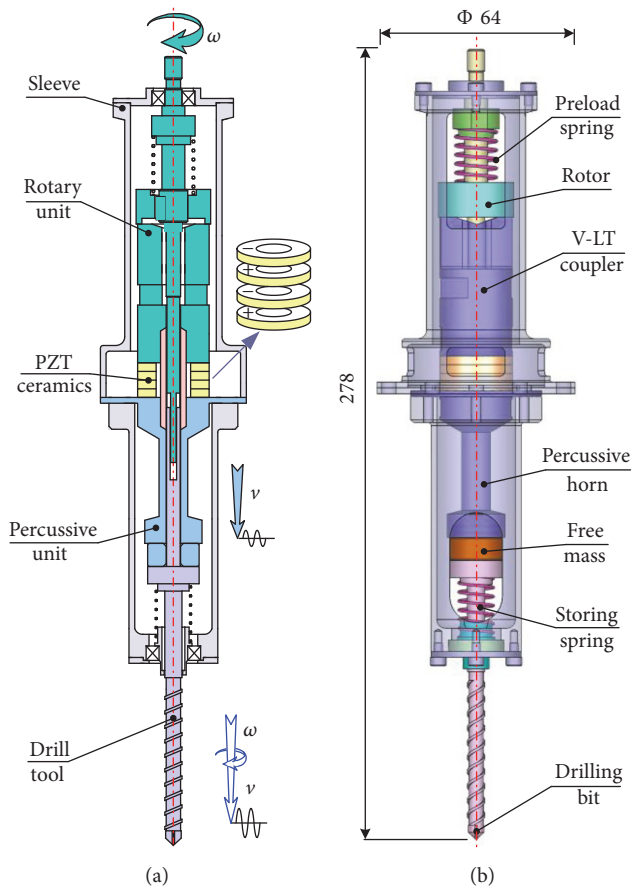

Figure 1: Structure of the RPUD.

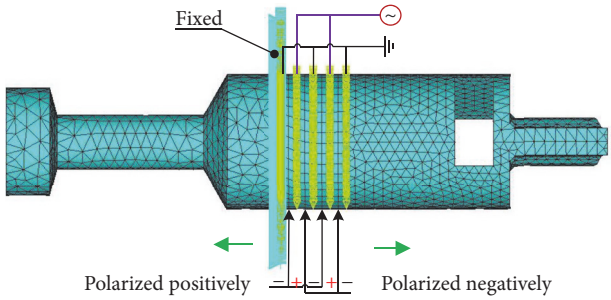

Figure 2: Finite element model of the rotary-percussive composition.

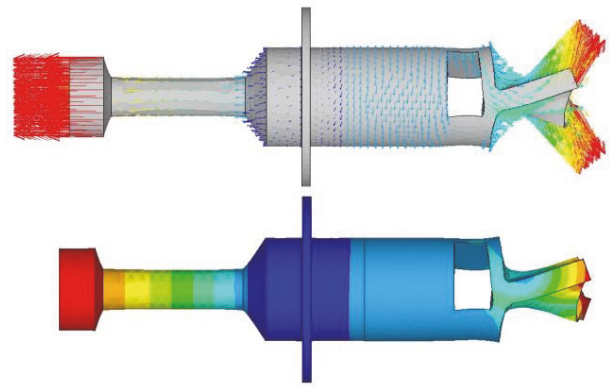

Figure 3: Modal analysis of the rotary-percussive composition.

the vibration modal analysis of the V-LT coupler and percussive horn is well matched with each other [25], and the maximum vibration value is reached simultaneously.

After being excited by the voltage, the PZT ceramics transfer vibration to both sides simultaneously. The rotary-percussive composition synchronously reaches the resonance state and drives the drill tool to realize the rotary-percussive motion, respectively. Figure 4 shows the detailed working principle of rotary unit and percussive unit. When the rotary unit receives the vibration from the PZT ceramics, V-LT coupler transforms longitudinal vibration into longitudinal-torsional vibration and an elliptical motion is formed on the top of driving teeth of the V-LT coupler. With the preload force provided by preload spring, friction is generated on the contact surface between the driving teeth and the rotor, which drives the rotor to rotate continuously. In the percussive unit, the percussive horn enlarges the longitudinal vibration from the PZT ceramics and passes the vibration to free mass. Then, the free mass transmits the percussive vibrating energy to the drill tool based on the continuous impact movement with the drill tool. Since the driving voltage changes in accordance

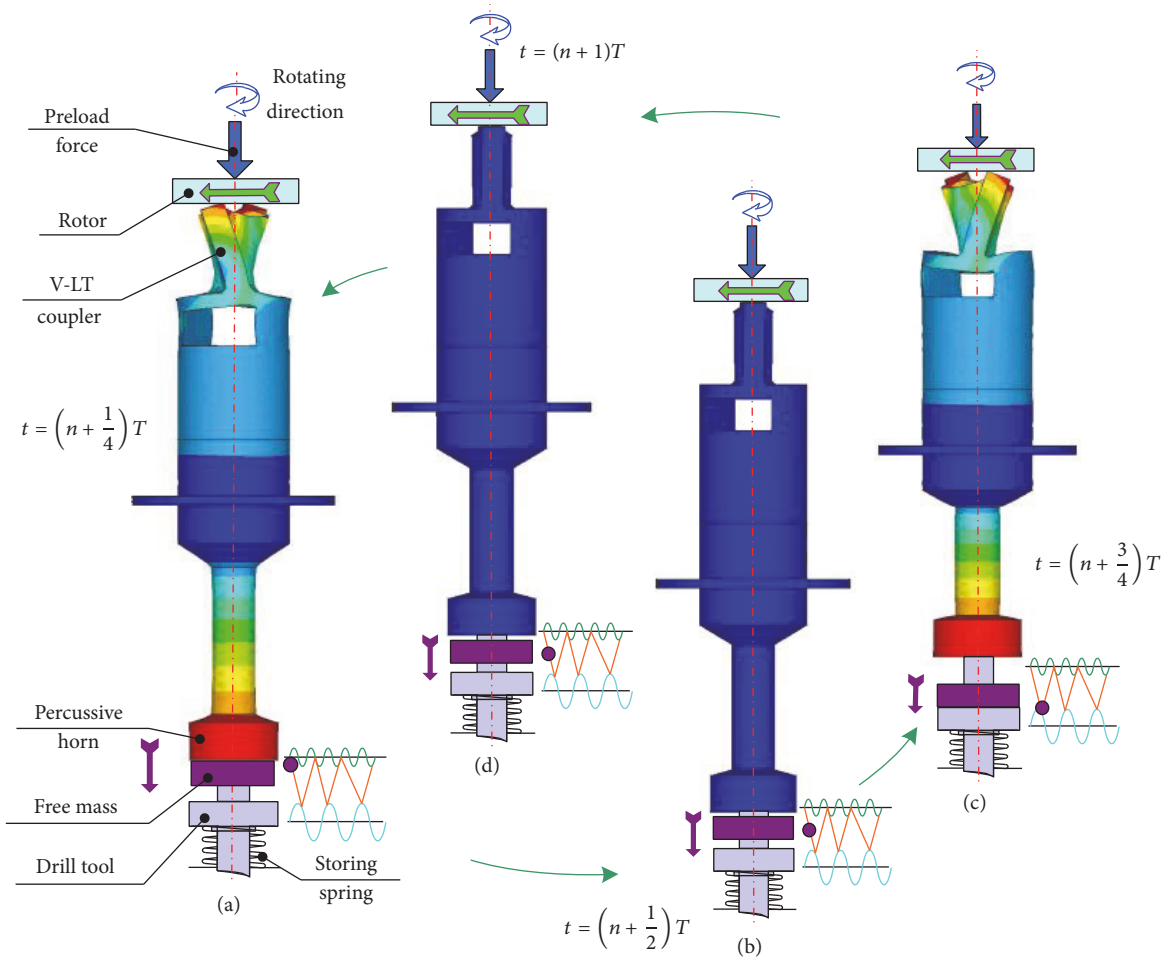

Figure 4: Working principle of rotary unit and percussive unit.

with the sinusoidal period, the rotary unit and the impact unit also drive the drill tool to carry out periodic movement, which follows the sequence of (a)-(b)-(c)-(d).

3. Collision Model of Percussive System

In the percussive system work process, after being excited by resonance voltage, the PZT ceramics generate a first longitudinal vibration mode and drive percussive horn which produces longitudinal vibration. As the percussive system is composed of the percussive horn, the free mass, and the drill tool, the percussive horn transmits vibrations at an ultrasonic frequency to the free mass, and then free mass delivers the vibration to the drill tool. The percussive motion of the drill tool is achieved by the collision process with the free mass. The collision of free mass is a highly nonlinear motion, which contains lots of influencing factors. In order to describe the motion of free mass more clearly, some secondary factors need to be ignored. So, some assumptions should be made before establishment of the free mass collision model.

(1) The PZT ceramics are fixed at the nodal plane, the displacement of percussive horn is a simple harmonic vibration, and the vibration process is not affected by the collision of free mass.

(2) The rotary-percussive ultrasonic drill works in no-load condition, and the drill tool can vibrate freely along the axial direction.

(3) In the collision modeling process, effect of friction force between the free mass, the percussive horn, and the drill tool is ignored.

(4) The centroid of the percussive horn, the free mass, and the drill tool are coaxial during the collision process.

(5) There is no aerodynamic drag, and the coefficient of restitution is a constant.

The collision process between the free mass, the percussive horn, and the drill tool is shown in Figure 5(a). Tip of the percussive horn makes a simple harmonic vibration under the driving of the PZT ceramics. The free mass vibrates between the percussive horn and the drill tool, passing the vibration energy. The modeling of the collision process between the free mass, the percussive horn, and the drill tool is shown in Figure 5(b). The top $u(t)$ is the displacement of the percussive horn, the bottom $v(t)$ is the displacement of the

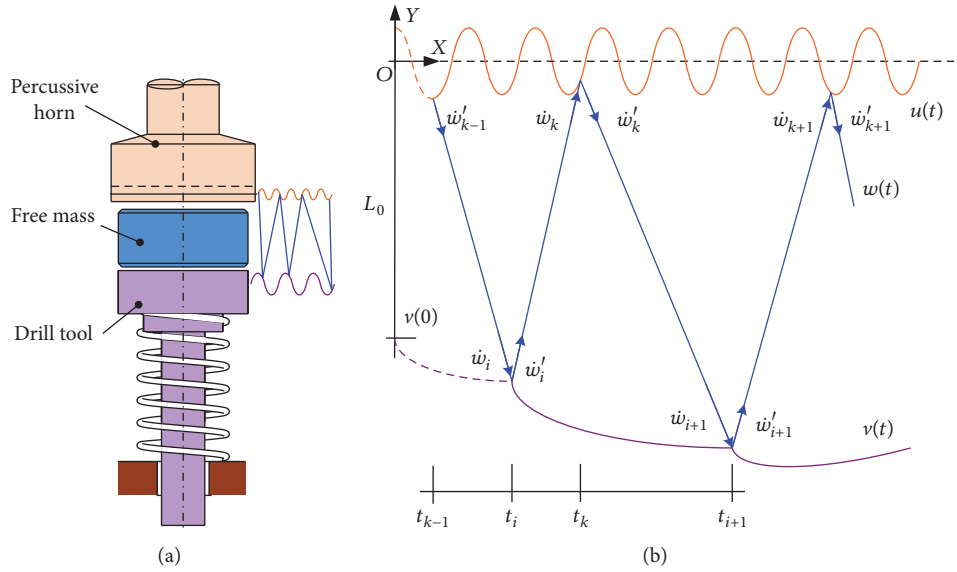

FIGURE 5: Collision model of free mass. (a) Composition of collision system. (b) Modeling of collision system.

drill tool, and the middle $w(t)$ is the vibration of the free mass. In the coordinate system the OX direction is the center line direction of the percussive horn vibration displacement, and the OY direction is the initial displacement direction of the percussive system. The initial interval between the percussive horn and the drill tool is L_0.

The motion of the percussive horn can be written as

$$u(t) = A_0 \cos(2\pi f t), \tag{1}$$

where A_0 is the vibration amplitude of percussive horn and f is the vibration frequency.

So, the velocity of the percussive horn can be given as

$$\dot{u}(t) = -2\pi f A_0 \sin(2\pi f t). \tag{2}$$

The initial time of the calculation is assumed to be t_{k-1}. After the collisionwith the percussive horn, the free mass velocity is $\dot{w}'_{k-1}$.

3.1. Calculation of the Collision Time between Free Mass and Drill Tool t_i. The vibration parameters of free mass at time of t_{k-1} can be written as

$$\begin{aligned} \ddot{w}(t) &= -g \\ w(t_{k-1}) &= u(t_{k-1}) \\ \dot{w}'(t_{k-1}) &= \dot{w}'_{k-1}, \end{aligned} \tag{3}$$

where g is acceleration of gravity. As one assumes the OY direction is positive, g is negative after t_{k-1}.

The vibration equation of free mass after t_{k-1} is

$$w(t) = u'_{k-1} - \frac{g}{2}(t - t_{k-1})^2 + \dot{w}'_{k-1}(t - t_{k-1}) \quad \forall t \in [t_{k-1}, t_i). \tag{4}$$

After t_{k-1}, free mass accelerates the velocity to the drill tool. And the velocity of the free mass can be given as

$$\dot{w}(t) = \dot{w}'_{k-1} - g(t - t_{k-1}) \quad \forall t \in [t_{k-1}, t_i). \tag{5}$$

In the percussive system, the motion of the drill tool is a free vibration with viscous damping. The equation of motion can be expressed as follows [26]:

$$\ddot{v}(t) + \frac{c}{m_v}\dot{v}(t) + \frac{k_0}{m_v}v(t) = 0, \tag{6}$$

where c is viscous damping coefficient of the drill tool and k_0 is equivalent stiffness coefficient of the drill tool.

The equation of motion of the drill tool before the t_ith collision can be written as

$$v_{i-1}(t) = \left[e^{-\zeta\omega_n t}\sin(\omega_d t + \varphi)\right]\sqrt{{v_{i-1}}^2 + \left(\frac{\dot{v}'_{i-1} + \zeta\omega_n v_{i-1}}{\omega_d}\right)^2} \quad \forall t \in (t_{i-1}, t_i], \tag{7}$$

where $\tan\varphi = \omega_d v_{i-1}/(\dot{v}'_{i-1} + \zeta\omega_n v_{i-1})$, $\omega_n = \sqrt{k_0/m_v}$, is the natural frequency of the drill tool without damping, $\omega_d = \sqrt{(1-\zeta^2)}\omega_n$, and $\zeta = c/2m_v\omega_n$.

At t_i moment, the contact condition of the free mass with the drill tool can be given by

$$v(t_i) = w(t_i). \tag{8}$$

That is,

$$\left[e^{-\zeta\omega_n t_i}\sin(\omega_d t_i + \varphi)\right]\sqrt{{v_{i-1}}^2 + \left(\frac{\dot{v}'_{i-1} + \zeta\omega_n v_{i-1}}{\omega_d}\right)^2} = u'_{k-1} - \frac{g}{2}(t_i - t_{k-1})^2 + \dot{w}'_{k-1}(t_i - t_{k-1}). \tag{9}$$

By solving (9) t_i is obtained. The velocity of the free mass and the drill tool before collision can be obtained by substituting t_i in the velocity equation of the free mass and the drill tool. The velocity can be expressed as

$$\begin{aligned}\dot{w}(t_i) &= \dot{w}'_{k-1} + \frac{g}{2}(t_i - t_{k-1})\\ \dot{v}(t_i) &= e^{-\zeta\omega_n t_i}\left[\omega_d \cos(\omega_d t_i + \varphi) - \zeta\omega_n \sin(\omega_d t_i + \varphi)\right]\\ &\cdot \sqrt{{v_0}^2 + \left(\frac{\dot{v}_0 + \zeta\omega_n v_0}{\omega_d}\right)^2}.\end{aligned} \tag{10}$$

The collision process of the free mass and the drill tool satisfies the momentum conservation theorem, which can be written as [27]

$$m_v \dot{v}(t) + m_w \dot{w}(t) = m_v \dot{v}'(t) + m_w \dot{w}'(t), \tag{11}$$

where m_v is the mass of the drill tool and m_w is the mass of the free mass.

The coefficient of restitution e_1 between the free mass and the drill tool can be given by [28]

$$e_1 = \frac{\dot{w}'_i - \dot{v}'_i}{\dot{v}_i - \dot{w}_i}. \tag{12}$$

So, the velocity of the free mass and the drill tool after collision of the time t_i can be expressed as

$$\begin{aligned}\dot{v}'(t_i) &= \dot{v}_i + \frac{m_w}{m_v + m_w}(1 + e_1)(\dot{w}_i - \dot{v}_i)\\ \dot{w}'(t_i) &= \dot{w}_i - \frac{m_v}{m_v + m_w}(1 + e_1)(\dot{w}_i - \dot{v}_i).\end{aligned} \tag{13}$$

3.2. Calculation of the Collision Time between Free Mass and Percussive Horn t_k. The vibration parameters of free mass at time of t_i can be written as

$$\begin{aligned}\ddot{w}(t) &= -g\\ w(t_i) &= v(t_i)\\ \dot{w}'(t_i) &= \dot{w}'_i.\end{aligned} \tag{14}$$

The vibration equation of free mass after t_i is

$$w(t) = v_i - \frac{g}{2}(t - t_i)^2 + \dot{w}'_i(t - t_i) \quad \forall t \in [t_i, t_k). \tag{15}$$

After t_i, free mass decelerates the velocity to the percussive horn. At t_k moment, the contact condition of the free mass with the percussive horn can be given by

$$u(t_k) = w(t_k). \tag{16}$$

That is,

$$\begin{aligned}&A_0 \cos(2\pi f t_k)\\ &= e^{-\zeta\omega_n t_i}\left[\omega_d \cos(\omega_d t_i + \varphi) - \zeta\omega_n \sin(\omega_d t_i + \varphi)\right]\\ &\cdot \sqrt{{v_0}^2 + \left(\frac{\dot{v}_0 + \zeta\omega_n v_0}{\omega_d}\right)^2} - \frac{g}{2}(t_k - t_i)^2\\ &+ \dot{w}'_i(t_k - t_i).\end{aligned} \tag{17}$$

By solving (17) t_k is obtained. The velocity of the free mass and the percussive horn before collision can be obtained by substituting t_k in the velocity equation of the free mass and the percussive horn. So, the velocity can be expressed as

$$\begin{aligned}\dot{w}(t_k) &= \dot{w}'_i - g(t_k - t_i)\\ \dot{u}(t_k) &= -2\pi f A_0 \sin(2\pi f t_k).\end{aligned} \tag{18}$$

The collision process of the free mass and the percussive horn satisfies the momentum conservation theorem, which can be given as

$$m_u \dot{u}(t_k) + m_w \dot{w}(t_k) = m_u \dot{u}'(t_k) + m_w \dot{w}'(t_k). \tag{19}$$

The coefficient of restitution e_2 between the free mass and the percussive horn can be given by

$$e_2 = \frac{\dot{w}'_k - \dot{u}'_k}{\dot{u}_k - \dot{w}_k}. \tag{20}$$

Considering that the percussive horn is the power source of the vibration system, it is assumed that the vibration of the horn is not affected by the collision process of the free mass. So, the velocity of the percussive horn and the free mass after collision of the time t_k can be expressed as

$$\begin{aligned}\dot{u}'(t_k) &= \dot{v}_k\\ \dot{w}'(t_k) &= \dot{w}_k - \frac{m_u}{m_u + m_w}(1 + e_2)(\dot{w}_k - \dot{u}_k).\end{aligned} \tag{21}$$

4. Analysis of Collision Model

In order to get a visual understanding of the collision process, MATLAB is employed for analysis of the collision model of the percussive horn, the free mass, and the drill tool. To obtain the numerical solution of collision model, the initial parameters of the collision system are given in Table 1. The collision process through time between the free mass, the percussive horn, and the drill tool is obtained through calculation.

Figure 6 shows the vibration displacement for the first 50 milliseconds of the percussive system. The vibration displacement for the first 20 milliseconds is shown in Figure 7. The vibration frequency of the free mass is varied during the collision process, and the average collision frequency of the free mass is about 520 Hz. As the free mass and the drill tool are coupled together by the collision process, the vibration

Table 1: The initial parameters of the percussive system.

Parameters	Symbols	Unit	Value
Acceleration of gravity	g	m/s^2	9.8
Coefficient of restitution between the free mass and the drill tool	e_1	—	0.8
Coefficient of restitution between the free mass and the percussive horn	e_2	—	0.9
Vibration amplitude of the percussive horn	A_0	μm	15
Vibration frequency of the percussive horn	f	kHz	20
Mass of percussive horn	m_u	kg	0.08
Mass of drill tool	m_v	kg	0.05
Mass of free mass	m_w	kg	0.008

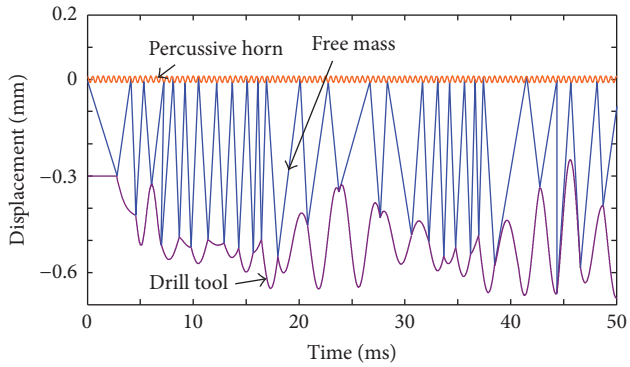

Figure 6: The vibration displacement for the first 50 milliseconds of the percussive system.

of the drill tool follows with the free mass, which changes the state of vibration after each collision. The free mass converts ultrasonic-frequency small-amplitude vibration of the percussive horn into a lower-frequency large-amplitude vibration of the drill tool through the collision process.

To analyze the effect of the free mass on the energy delivering process, the kinetic energy of the drill tool is calculated after collision with different weight of free mass, as shown in Figures 8(a)–8(d). It is observed that, with the weight of free mass changed from 2 g to 8 g, the kinetic energy of the drill tool after collision is also increased, and the increase of kinetic energy is linear with the weight of free mass.

5. Experiments

To verify the calculation results of the collision model, high-speed camera system and drilling experiments are employed to evaluate the vibration process of the percussive system.

5.1. Vibration Measurement Using High-Speed Camera System. High-speed camera is a device for recording fast-moving motion, which can measure the movement state of objects [29]. To verify the collision model result, this paper uses the high-speed camera to measure the vibration process and analyze the nonlinear dynamic behavior of the free mass

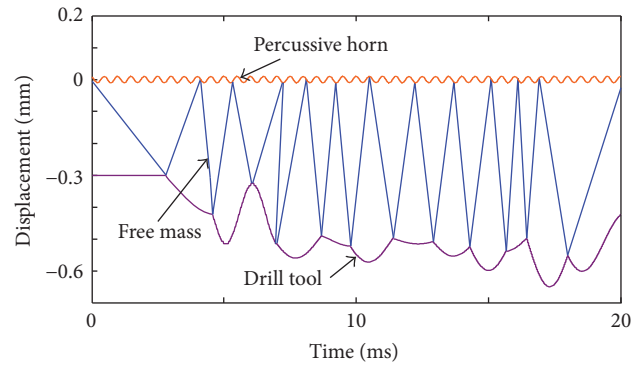

Figure 7: The vibration displacement for the first 20 milliseconds of the percussive system.

with percussive horn and drill tool. The test uses Phantom V12 high-speed camera, as shown in Figure 9(a). In order to match the requirements of the tracking of free mass movement, the camera parameter of the high-speed camera is set to 5000 frames per second. Before test, it is necessary to identify the percussive horn, the free mass, and the drill tool, as shown in Figure 9(b). High-speed camera is used to measure the percussive motion of the free mass between the percussive horn and the drill tool. The displacement and vibration velocity of free mass are extracted, respectively, as shown in Figures 10 and 11. The maximum displacement of free mass is nearly 6 mm and the maximum vibration velocity is nearly 80 mm/s. In order to determine the frequency range of the free mass in the collision process, Fourier transform is performed on the time domain characteristics of the displacement of free mass. The corresponding frequency spectrum is obtained, as shown in Figure 12. According to the spectrum, the vibration frequency of the free mass is mostly in the range of 0~400 Hz, which is consistent with the previous theoretical analysis result.

To validate the effect of the weight of free mass on the percussive energy of the drill tool in the collision model, different weights of free masses are assembled into the RPUD, and the vibration velocity of the drill tool is measured with the help of the high-speed camera system. The average kinetic energy of the drill tool is measured and compared with the theoretical results in the collision model, as shown in Figure 13. With the weight of free mass changed from 0 g to 8 g, the theoretical values and measured values of the kinetic energy of drill tool are gradually increased. It can be inferred that the larger the weight of the free mass, the greater the percussive kinetic energy delivered to the drill tool, which verifies the aforementioned collision model calculation results in Figure 8.

5.2. Drilling Experiments. To further observe the effect of the free mass on the percussive kinetic energy of the drill tool, drilling experiments of RPUD with load condition is carried out under different weights of free mass. To keep the rationality of drilling experiments, RPUD operates at both rotary-percussive mode and percussive mode. The drilling experiments are accomplished under exciting voltage of

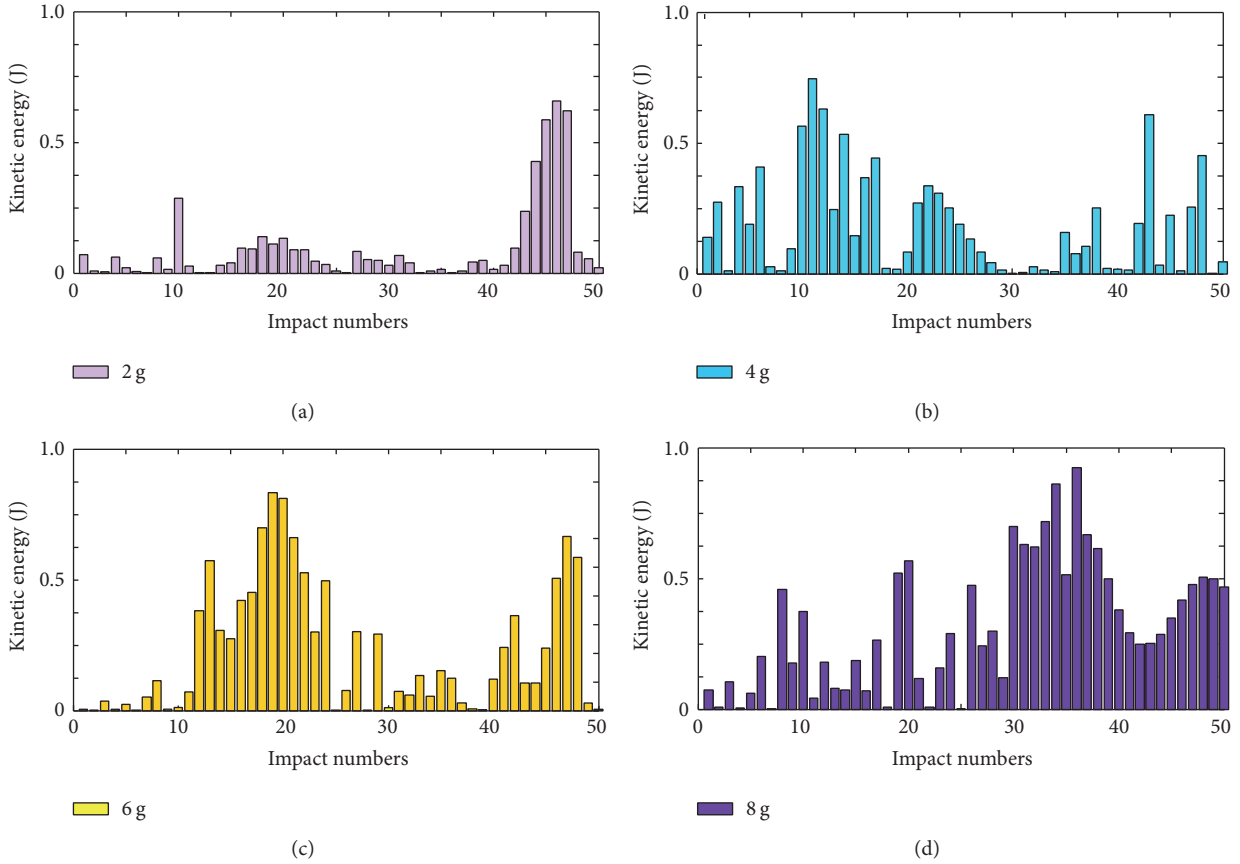

Figure 8: The kinetic energy of the drill tool after collision under different weights of free mass.

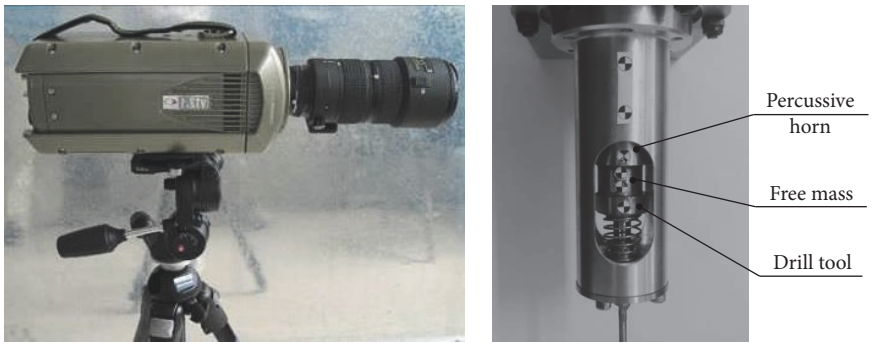

(a) High-speed camera (b) Marked percussive system

Figure 9: Vibration measurement using high-speed camera system. (a) Phantom V12 high-speed camera. (b) Marked percussive system.

225 V and exciting frequency of 19.95 kHz. Diameter of drill tool is 3 mm, the drilling time is 5 minutes, the weight on bit is 7 N, the drilling object is sandstone, and the drilling depth is observed under different weights of free mass, as shown in Figure 14.

The rotary-percussive drilling and percussive drilling results show that the drilling depth increases with the weight of free mass from 0 g to 8 g. As the weight becomes 8 g, the drilling depth reaches the maximum value. This is consistent with the previous high-speed camera vibration measurement results. The experiments also indicate that rotary-percussive drilling has higher drilling efficiency than percussive drilling, which validates the aforementioned advantages of the RPUD.

6. Conclusions

This paper proposed an impact dynamics analysis of the percussive system based on the rotary-percussive ultrasonic

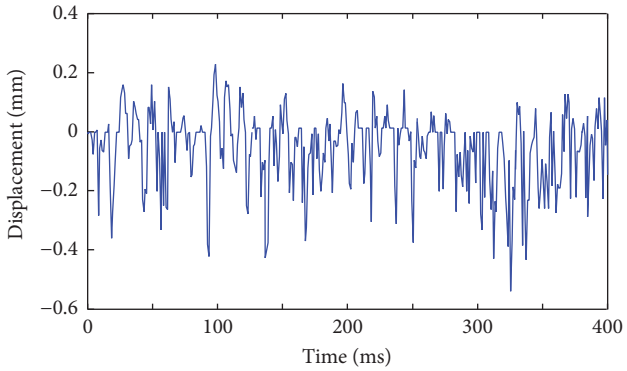

Figure 10: The vibration displacement of free mass.

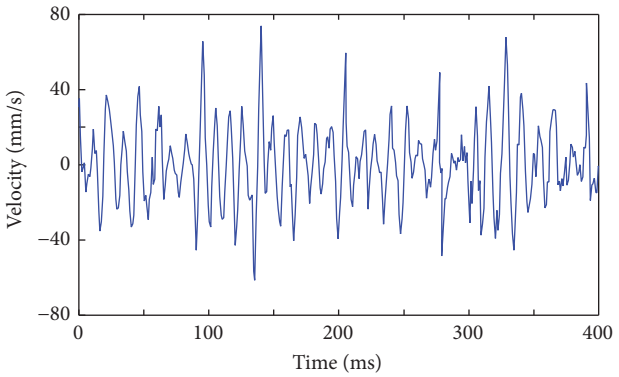

Figure 11: The vibration velocity of free mass.

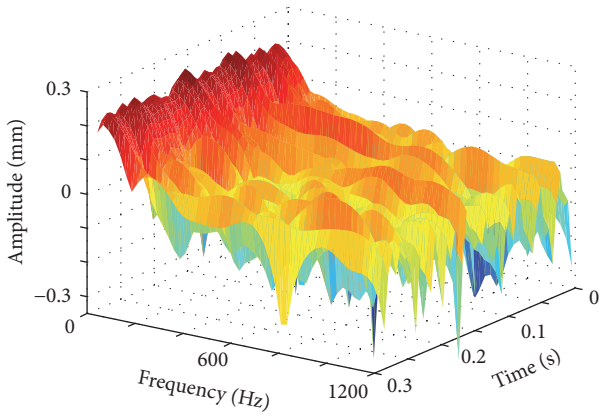

Figure 12: The corresponding frequency spectrum of free mass.

drill (RPUD). The proposed RPUD uses the vibrations on two sides of one single piezoceramic, with achieved rotary-percussive motion, which has higher drilling efficiency compared with percussive ultrasonic drill. The theory of conservation of momentum and Newton's impact law are employed to analyze the collision process of the percussive system under no-load condition. The collision process of the free mass between the percussive horn and the drill tool is analyzed, and the effect of the weight of free mass on the kinetic energy of drill tool is discussed as well. High-speed camera system and drilling experiments are used to verify the analysis results.

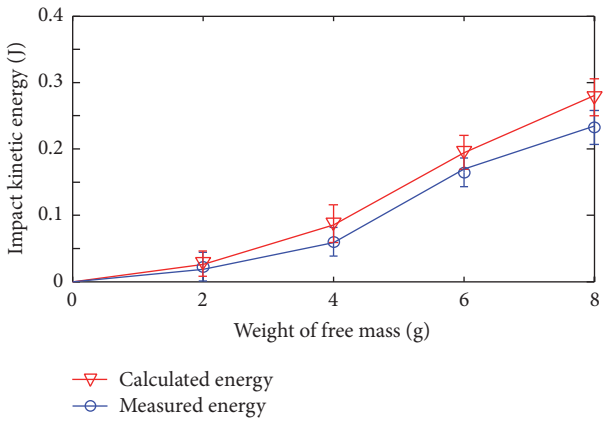

Figure 13: The average kinetic energy of the drill tool in theoretical results and measured results.

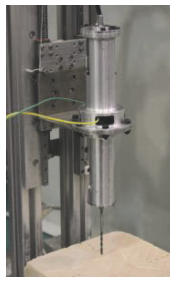

Test bed of RPUD

(a)

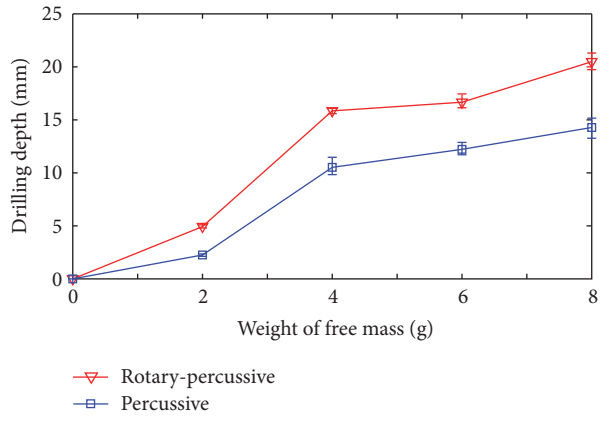

(b)

Figure 14: Drilling experiment of RPUD. (a) Test bed of RPUD. (b) Drilling depth of RPUD under different weight of free mass.

In the collision process of the percussive system, the free mass transmits high-frequency small-amplitude vibration of the percussive horn into low-frequency large-amplitude vibration and delivers the impact energy to the drill tool which achieved the percussive movement of the drill tool. In the range of RPUD drive capability, increasing the weight of the free mass can effectively raise the kinetic energy of the drill tool during collision process.

Conflicts of Interest

The authors declare no conflicts of interest.

Acknowledgments

The project is financially supported by fundamental research funds for National Natural Science Foundation of China (61403106).

References

[1] K. Zacny, Y. Bar-Cohen, M. Brennan et al., "Drilling systems for extraterrestrial subsurface exploration," *Astrobiology*, vol. 8, no. 3, pp. 665–706, 2008.

[2] Y. Bar-Cohen and K. Zacny, "Drilling in Extreme Environments," *Chapter Extraterrestrial Drilling and Excavation*, pp. 347–546, 2008.

[3] K. Zacny, J. Wilson, P. Chu, and J. Craft, "Prototype rotary percussive drill for the Mars sample return mission," in *Proceedings of the proceeding of the 2011 IEEE Aerospace Conference, AERO '11*, 9 pages, Montana, MT, USA, March 2011.

[4] Z. Y. Ouyang, "Scientific objectives of Chinese lunar exploration project and development strategy," *Advance in Earth Sciences*, vol. 19, pp. 351–358, 2004.

[5] P. Harkness and M. Lucas, "A brief overview of space applications for ultrasonics," *Ultrasonics*, vol. 52, no. 8, pp. 975–979, 2012.

[6] Y. Bar-Cohen, S. Sherrit, B. P. Dolgin et al., "Ultrasonic/sonic driller/corer (USDC) as a sampler for planetary exploration," *IEEE Aerospace Conference Proceedings*, vol. 1, pp. 1263–1271, 2001.

[7] X. Bao, Y. Bar-Cohen, Z. Chang et al., "Modeling and computer simulation of ultrasonic/sonic driller/corer (USDC)," *IEEE Transactions on Ultrasonics, Ferroelectrics, and Frequency Control*, vol. 50, no. 9, pp. 1147–1160, 2003.

[8] M. Badescu, X. Bao, Y. Bar-Cohen, Z. Chang, and S. Sherrit, "Integrated modeling of the ultrasonic/sonic drill/corer - Procedure and analysis results," in *Proceedings of the Smart Structures and Materials 2005 - Smart Structures and Integrated Systems*, pp. 312–323, March 2005.

[9] P. N. H. Thomas, "Magna Parva and ESA's ultrasonic drill tool for planetary surface exploration," in *Proceedings of the 12th International Conference on Engineering, Science, Construction, and Operations in Challenging Environments - Earth and Space 2010*, pp. 1235–1245, March 2010.

[10] Q. Quan, H. Li, S. Jiang, Z. Deng, X. Hou, and D. Tang, "A piezoelectric-driven ultrasonic/sonic driller for planetary exploration," in *Proceedings of the 2013 IEEE International Conference on Robotics and Biomimetics, ROBIO 2013*, pp. 2523–2528, December 2013.

[11] A. Cardoni, P. Harkness, and M. Lucas, "Ultrasonic rock sampling using longitudinal-torsional vibrations," *Physics Procedia*, vol. 3, no. 1, pp. 125–134, 2010.

[12] M. Badescu, S. Sherrit, X. Bao, Y. Bar-Cohen, and B. Chen, "Auto-Gopher - A wire-line rotary-hammer ultrasonic drill," in *Proceedings of the Sensors and Smart Structures Technologies for Civil, Mechanical, and Aerospace Systems 2011*, March 2011.

[13] K. Zacny, G. Paulsen, Y. Bar-Cohen et al., "Wireline deep drill for exploration of Mars, Europa, and Enceladus," in *Proceedings of 2013 IEEE Aerospace Conference, AERO 2013*, March 2013.

[14] M. Badescu, J. Hasenoehrl, Y. Bar-Cohen et al., "Percussive augmenter of rotary drills (PARoD)," in *Proceedings of the SPIE Smart Structures and Materials + Nondestructive Evaluation and Health Monitoring*, p. 86921Q, San Diego, Calif, USA.

[15] X. Li, K. Worrall, P. Harkness et al., "A Motion Control System Design for an Ultrasonic Planetary Core Drill (UPCD) Unit," in *in Proceedings of AIAA SPACE 2015 Conference and Exposition*, pp. 1–11, Pasadena, Calif, USA, June 2015.

[16] R. Timoney, P. Harkness, X. Li, A. Bolhovitins, A. Cheney, and M. Lucas, "The Development of the European UItrasonic Planetary Core Drill (UPCD)," in *Proceedings of the AIAA SPACE 2015 Conference and Exposition*, Pasadena, Calif, USA.

[17] S. Sherrit, L. Domm, X. Bao, Y. Bar-Cohen, and Z. Chang, "Single piezo-actuator rotary-hammering (SPaRH) drill," in *Proceedings of the Sensors and Smart Structures Technologies for Civil, Mechanical, and Aerospace Systems 2012*, San Diego, Calif, USA, March 2012.

[18] Y. Wang, H. Li, D. Bai et al., "A rotary-percussive ultrasonic drill for planetary rock sampling," in *Proceedings of the 2016 IEEE/RSJ International Conference on Intelligent Robots and Systems, IROS 2016*, pp. 2966–2971, October 2016.

[19] N. Neumann, T. Sattel, and J. Wallaschek, "On the Analysis of a Simple Impact Drill Model using Set-Oriented Numerical Methods," *PAMM*, vol. 5, no. 1, pp. 119-120, 2005.

[20] N. Neumann and T. Sattel, "Set-oriented numerical analysis of a vibro-impact drilling system with several contact interfaces," *Journal of Sound and Vibration*, vol. 308, no. 3-5, pp. 831–844, 2007.

[21] L. J. Vila and R. B. Malla, "Analytical model of the contact interaction between the components of a special percussive mechanism for planetary exploration," *Acta Astronautica*, vol. 118, pp. 158–167, 2016.

[22] P. Harkness, M. Lucas, and A. Cardoni, "Architectures for ultrasonic planetary sample retrieval tools," *Ultrasonics*, vol. 51, no. 8, pp. 1026–1035, 2011.

[23] A. Kumada, "A piezoelectric ultrasonic motor," *Japanese Journal of Applied Physics*, vol. 24, pp. 739–741, 1985.

[24] T. Stolarski, Y. Nakasone, and S. Yoshimoto, "Engineering analysis with ANSYS software," in *Chapter Mode Analysis*, pp. 143–185, 2011.

[25] Y. Liu, X. Yang, W. Chen, and D. Xu, "A Bonded-Type Piezoelectric Actuator Using the First and Second Bending Vibration Modes," *IEEE Transactions on Industrial Electronics*, vol. 63, no. 3, pp. 1676–1683, 2016.

[26] D. E. Newland, *Mechanical vibration analysis and computation*, vol. 4, Courier Corporation, 2013.

[27] R. M. Brach, "Mechanical impact dynamics: rigid body collisions," *Chapter Vibratory Impact*, pp. 189–206, 1991.

[28] G. Gilardi and I. Sharf, "Literature survey of contact dynamics modelling," *Mechanism and Machine Theory*, vol. 37, no. 10, pp. 1213–1239, 2002.

[29] H.-H. Kim, J.-H. Kim, and A. Ogata, "Time-resolved high-speed camera observation of electrospray," *Journal of Aerosol Science*, vol. 42, no. 4, pp. 249–263, 2011.